

Revealing the intricate dune-dune interactions of bidisperse barchans

W. R. Assis¹, F. D. Cúñez², E. M. Franklin¹

¹School of Mechanical Engineering, UNICAMP - University of Campinas, Rua Mendeleyev, 200,
Campinas, SP, Brazil

²Department of Earth and Environmental Sciences, University of Rochester, Rochester, NY 14627, USA

Key Points:

- Barchan-barchan interactions in the presence of two species of grains vary with their concentrations
- We found different structures, including a collision in which the upstream barchan is the largest
- We propose a timescale for the interactions of both monodisperse and bidisperse barchans

Abstract

Three dimensional dunes of crescentic shape, called barchans, are commonly found on Earth and other planetary environments. In the great majority of cases, barchans are organized in large fields in which corridors of size-selected barchans are observed, and where barchan-barchan interactions play an important role in size regulation. Previous studies shed light on the interactions between barchans by making use of monodisperse particles, but dunes in nature consist, however, of polydisperse grains. In this paper, we investigate the binary interactions of barchans consisting of (i) bidisperse mixtures of grains and (ii) different monodisperse grains (one type for each barchan). We performed experiments in a water channel where grains of different sizes were poured inside forming two barchans that interacted with each other while filmed by a camera, and we obtained their morphology from image processing. We observed that a transient stripe appears over the dunes in cases of bidisperse mixtures, that interaction patterns vary with concentrations, and that different interactions exist when each barchan consists of different monodisperse grains. Interestingly, we found the conditions for a collision in which the upstream barchan is larger than the downstream one, and we propose a timescale for the interactions of both monodisperse and bidisperse barchans. Our results represent a new step toward understanding complex barchanoid structures found on Earth, Mars and other celestial bodies.

Plain Language Summary

Barchans are crescent-shaped dunes commonly found in dune fields on Earth and other planetary environments, and it has been shown that their sizes are highly influenced by barchan-barchan interactions. The composition of the granular bed can affect the observed patterns and sizes, but had not been investigated until now. Because those interactions take long times to be completed in gaseous environments (estimated in decades and millenniums for aeolian and Martian dunes, respectively) when compared with the aquatic case (of the order of minutes), we performed experiments in a water channel where bidisperse grains (in terms of size) were poured inside, forming two barchans that interacted with each other. We found different structures, including a collision in which the upstream barchan is the largest, and propose a general timescale for the interactions of both monodisperse and bidisperse barchans. The identification of such timescale represents a new step for predicting the duration of binary interactions and, more generally, scaling the evolution of dune fields on Earth, Mars and other planetary environments.

1 Introduction

Under one-directional fluid flow and limited amount of sand, three dimensional dunes of crescentic shape, called barchans, consistently grow (Bagnold, 1941; Herrmann & Sauer- mann, 2000; Hersen, 2004), being commonly found on Earth, Mars, other celestial bodies (Elbelrhiti et al., 2005; Claudin & Andreotti, 2006; E. J. R. Parteli & Herrmann, 2007). In the great majority of cases, barchans are organized in large fields in which corridors of size-selected barchans are observed, and where barchan-barchan interactions play an important role in size regulation (Hersen et al., 2004; Hersen & Douady, 2005; Kocurek et al., 2010; Génois, Hersen, et al., 2013; Génois, du Pont, et al., 2013; Assis & Franklin, 2020, 2021). Given the ubiquitous nature of barchans, understanding how their shape is formed, how they self organize in regular fields, and how they are affected by the bed granulometry are of paramount importance to deduce the past and predict the future of barchans on Earth and other planetary environments.

Several studies investigated the interactions between barchans, shedding light on certain aspects of barchan-barchan interactions, but leaving many others, however, poorly understood. Among the drawbacks of previous studies, field measurements were very limited in time, since aeolian barchans take decades to complete interact with each other

64 (Bagnold, 1941; Hersen et al., 2002), and previous experimental and numerical studies
65 made use of monodisperse particles, whereas dunes in nature consist of polydisperse grains.
66 Therefore, one way to overcome those drawbacks is by carrying out experiments with
67 polydisperse grains under water, the subaqueous barchans being much faster and smaller
68 than the aeolian dunes (the former having characteristic times and lengths of minutes
69 and centimeters, e.g., Hersen et al., 2002; Franklin & Charru, 2009, 2011; Alvarez & Franklin,
70 2017).

71 Field measurements of aeolian barchan-barchan interactions are of course impor-
72 tant, consisting in a direct observation of nature, and past studies showed that the col-
73 lisions of barchans regulate their size and generate different barchanoid forms (Norris
74 & Norris, 1961; Gay, 1999; Vermeesch, 2011; Elbelrhiti et al., 2008; Hugenholtz & Barchyn,
75 2012). However, the time series are frequently incomplete (given the large timescales in-
76 volved), and, therefore, numerical and experimental investigations have been conducted
77 in parallel with field experiments.

78 The numerical studies made use of continuum (Schwämmle & Herrmann, 2003; Durán
79 et al., 2005; Zhou et al., 2019) and discrete (Katsuki et al., 2011) models to compute the
80 evolution of a bed surface into a dune field, most of them incorporating rules for barchan-
81 barchan interactions (Lima et al., 2002; E. Parteli & Herrmann, 2003; Katsuki et al., 2005;
82 Durán et al., 2009). In addition to these techniques, Durán et al. (2009) and Génois, du
83 Pont, et al. (2013) proposed an agent-based model that makes use of sand flux balances
84 and elementary rules for barchan collisions, and Bo and Zheng (2013) used a scale-coupled
85 model (Zheng et al., 2009) to obtain the probability of occurrence of different types of
86 barchan-barchan collisions. Those numerical investigations showed that barchan-barchan
87 collisions lead to corridors of size-selected barchans, pointing toward homogeneous fields.
88 However, model simplifications prevented them from reproducing correctly all barchan-
89 barchan interactions, and, in addition, there is a lack of numerical studies at the grain
90 scale.

91 The experiments were carried out almost exclusively in water tanks and channels.
92 Some studies measured the flow disturbances caused by an upstream barchan upon a down-
93 stream one, such as done by Bristow et al. (Bristow et al., 2018, 2019, 2020), who found,
94 among other findings, that turbulence levels increase on the stoss surface of the down-
95 stream dune, enhancing erosion over the downstream dune. Other investigations mea-
96 sured the evolution of two interacting bedforms, identifying different interaction patterns
97 (Endo et al., 2004; Hersen & Douady, 2005; Bacik et al., 2020; Assis & Franklin, 2020)
98 and mass exchanges at the grain scale (Assis & Franklin, 2021). Endo et al. (2004) in-
99 vestigated collisions of aligned barchans by varying their mass ratio while maintaining
100 fixed the water flow rate, initial conditions and grain types, and they found three col-
101 lision patterns which were called merging, exchange and fragmentation-chasing by Assis
102 and Franklin (2020) (and explained next). Hersen and Douady (2005) investigated the
103 collisions of off-centered barchans by varying their transverse distances while keeping the
104 other parameters fixed, and showed that collisions produce smaller barchans, regulat-
105 ing thus their size when in a barchan field. The experiments of Bacik et al. (2020) were
106 devoted to the interaction over long times between a pair of two-dimensional dunes in
107 a circular channel, and they found that turbulent structures of the disturbed flow pre-
108 vent dune collisions by inducing dune-dune repulsion. Recently, Assis and Franklin (2020,
109 2021) inquired further into the binary interactions of subaqueous barchans by conduct-
110 ing experiments in both aligned and off-centered configurations where the water flow rates,
111 grain types (diameter, density and roundness), pile masses, longitudinal and transverse
112 distances, and initial conditions were varied, and measurements were made at the bed-
113 form and grain scales. They found five interaction patterns for both aligned and off-centered
114 configurations, proposed classification maps, measured the trajectories of individual grains
115 during barchan-barchan interactions, and found the typical lengths and velocities of grains,
116 the mass exchanged between barchans, and a diffusive length for some collisions.

117 From the previous works, the most comprehensive classification of barchan-barchan
 118 interactions is the one presented in Assis and Franklin (2020), which identifies: (i) chas-
 119 ing, when collision does not occur, the upstream barchan not reaching the downstream
 120 one; (ii) merging, when collision occurs and the dunes merge; (iii) exchange, when, once
 121 collision takes place, a small barchan is ejected; (iv) fragmentation-chasing, when the down-
 122 stream dune splits without collision taking place and the downstream bedforms outrun
 123 the upstream one; and (v) fragmentation-exchange, when fragmentation initiates, col-
 124 lision takes place, and a small barchan is ejected. The question that persists is if the same
 125 patterns and classification maps proposed by Assis and Franklin (2020) remain valid for
 126 aeolian and Martian barchans (and also other planetary environments), and polydisperse
 127 dunes. While proving the validity for aeolian and Martian barchans is hindered by their
 128 large timescales, that for polydisperse barchans, on the other hand, can be investigated
 129 in the subaqueous case.

130 Concerning dunes of polydisperse grains, Alvarez et al. (2021) investigated exper-
 131 imentally the growth of subaqueous single barchans consisting of bidisperse grains. In
 132 their experiments, single granular piles consisting of bidisperse mixtures in terms of grain
 133 sizes and/or densities were developed into barchan dunes, and they found that denser,
 134 smaller, and smaller and less dense grains tend to accumulate over the barchan surface.
 135 They also found that a transient stripe transverse to the flow direction appears just up-
 136 stream the crest of the initial bedform and migrates toward its leading edge until dis-
 137 appearing, that that line separates a downstream region where segregation is complete
 138 from the upstream region where segregation is still occurring, and that the final barchan
 139 morphology is roughly the same as that of monodisperse barchans. Finally, they proposed
 140 that segregation patterns result from a competition between fluid entrainment and eas-
 141 iness of rolling, and showed that grains segregate with a diffusion-like mechanism.

142 In this paper, we investigate the binary interactions of barchans when grains of two
 143 different sizes are involved. For that, we inquired into two specific cases: (i) each bed-
 144 form consisting of bidisperse mixtures; (ii) each bedform consisting of a given, but dif-
 145 ferent between them, grain type (two-species monodisperse barchans). The experiments
 146 were conducted in a water channel where grains were poured inside, forming two con-
 147 ical piles that were afterward deformed by the water flow into barchans that interacted
 148 with each other. The evolution and interactions of bedforms were recorded by a conven-
 149 tional camera and their morphology was obtained from image processing. We observe
 150 that a transient stripe appears over the dunes in cases of bidisperse mixtures (just as hap-
 151 pens for single bidisperse barchans (Alvarez et al., 2021)), that interaction patterns vary
 152 with concentrations, and that different interactions exist when each barchan consists of
 153 monodisperse grains of different kind (two-species monodisperse barchans), including col-
 154 lisions in which the upstream barchan is larger than the downstream one. Finally, we
 155 propose a timescale for the interactions of both monodisperse (one-species) and bidis-
 156 perse (cases i and ii) barchans. Our results represent a new step toward understanding
 157 complex barchanoid structures found on Earth, Mars and other celestial bodies.

158 In the following, Section 2 describes the experimental setup and procedure, Sec-
 159 tion 3 presents the obtained results, and Section 4 presents the conclusions.

160 2 Experimental Setup

161 The experimental device consisted basically of a water tank, centrifugal pumps, a
 162 flow straightener, a 5-m-long closed-conduit channel, a settling tank, and a return line,
 163 so that we imposed a pressure-driven water flow in closed loop. The channel had a rect-
 164 angular cross section 160 mm wide by $2\delta = 50$ mm high, was made of transparent ma-
 165 terial, and consisted of a 3-m-long entrance section (corresponding to 40 hydraulic di-
 166 ameters), a 1-m-long test section, and a 1-m-long section connecting the test section to
 167 the channel exit. With the channel filled with water in still conditions, controlled grains

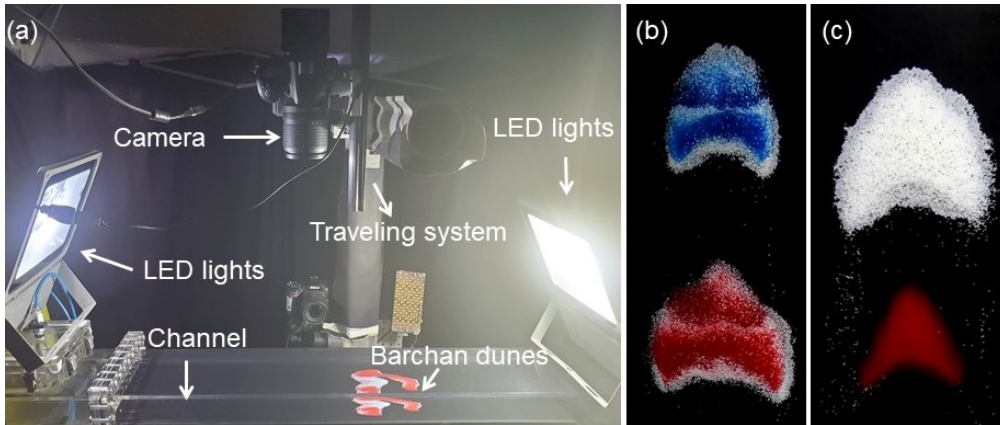


Figure 1. (a) Photograph of test section showing the dunes, camera and LED lights; (b) top-view image of two interacting bidisperse barchans (case *e* of Table 1); (c) top-view image of two interacting monodisperse barchans of different granulometry (case *o* of Table 1, of a larger barchan reaching a smaller one); In figures (b) and (c) the flow is from top to bottom.

168 were poured inside in order to form two aligned piles consisting of (i) bidisperse mixtures;
 169 (ii) different monodisperse grains (two-species, each pile consisting of one single species).
 170 Afterward, a specified water flow was imposed, deforming each pile into a barchan dune
 171 that interacted with each other while a camera recorded top view images of the bedforms.
 172 No influx of grains coming from regions upstream the test section was imposed and, there-
 173 fore, the entire system decreased in mass along time. Using the same terminology of pre-
 174 vious works (Assis & Franklin, 2020, 2021), we call *impact barchan* the one that was ini-
 175 tially upstream and *target barchan* the one that was initially downstream. Figure 1a shows
 176 a photograph of the test section, and Figures 1b and 1c top-view images of two inter-
 177 acting barchans consisting each of bidisperse and monodisperse grains, respectively. The
 178 layout of the experimental device is shown in the supporting information.

179 In our tests, we used tap water at temperatures within 22 and 28 °C and round
 180 glass beads ($\rho_s = 2500 \text{ kg/m}^3$) with diameters $0.15 \text{ mm} \leq d_{s1} \leq 0.25 \text{ mm}$ and 0.40 mm
 181 $\leq d_{s2} \leq 0.60 \text{ mm}$, which we call species 1 and 2, respectively. We consider in our com-
 182 putations the mean values $d_1 = 0.2 \text{ mm}$ and $d_2 = 0.5 \text{ mm}$ of d_{s1} and d_{s2} , respectively,
 183 and we used grains of different colors (white, red and blue) in order to track the differ-
 184 ent species along images (see the supporting information for microscopy images of the
 185 used grains). We varied the concentration of each grain type (ϕ_1 and ϕ_2) between 0 and
 186 1, the mass ratio of the piles (initial mass of the impact barchan m_i divided by that of
 187 the target one m_t) between 0.02 and 4, and the water velocities within $0.278 \text{ m/s} \leq U$
 188 $\leq 0.347 \text{ m/s}$, where U is the cross-sectional mean velocity of water. These values corre-
 189 spond to Reynolds numbers based on the channel height, $\text{Re} = \rho U 2\delta / \mu$, within $1.39 \times$
 190 10^4 and 1.74×10^4 , where μ is the dynamic viscosity and ρ the density of the fluid. We
 191 computed shear velocities of the undisturbed water flow over the channel walls u_* from
 192 measurements with a two-dimensional two-component particle image velocimetry (2D2C-
 193 PIV) device, and we use u_* as a reference value for fluid shearing even when bedforms
 194 are present in the channel. Our measurements show values within 0.0159 and 0.0193 m/s
 195 and that u_* follows the Blasius correlation (Schlichting, 2000). With those values, the
 196 Shields number $\theta = (\rho u_*^2) / ((\rho_s - \rho)gd)$ varied within 0.034 and 0.127 (where g is the
 197 acceleration of gravity). Table 1 summarizes the tested conditions, and complete tables
 198 with all the parameters (in dimensional form) are available on an open repository (Assis
 199 et al., 2021).

200 A digital camera with a lens of 18-140 mm focal distance and F2.8 maximum aper-
 201 ture was mounted on a traveling system in order to have a top view of the bedforms, and
 202 lamps of light-emitting diode (LED) were used as light source. The camera was of com-
 203plementary metal-oxide-semiconductor (CMOS) type with a maximum resolution of 1920
 204 px \times 1080 px at 60 Hz, and the region of interest (ROI) was set between 1311 px \times 451
 205 px and 1920 px \times 771 px, for fields of view varying within 354 mm \times 122 mm and 507
 206 mm \times 122 mm. The acquired images were afterward processed by numerical scripts that
 207 identified and tracked bedforms and patterns, and were based on Crocker and Grier (1996).
 208 Movies showing collisions of bidisperse barchans are available in the supporting infor-
 209 mation and on an open repository (Assis et al., 2021).

210 3 Results and discussion

211 3.1 Bidisperse piles

Case	ϕ_{1t}	ϕ_{2t}	ϕ_{1i}	ϕ_{2i}	D_t	D_i	Δx_d	Re	u_*	m_i/m_t	t_s	t_c	Pat
...	mm	mm	mm	...	mm/s	...	s
a	0.5	0.5	0.5	0.5	63	18	18	1.56×10^4	0.0176	0.02	230	0.1	M
b	0.5	0.5	0.5	0.5	61	24	23	1.56×10^4	0.0176	0.05	450	0.2	E
c	0.5	0.5	0.5	0.5	56	27	20	1.56×10^4	0.0176	0.11	499	0.6	FE
d	0.5	0.5	0.5	0.5	43	30	30	1.56×10^4	0.0176	0.43	1537	∞	FC
e	0.5	0.5	0.5	0.5	52	48	39	1.56×10^4	0.0176	0.67	10637	∞	C
f	0.8	0.2	0.8	0.2	56	22	21	1.56×10^4	0.0176	0.05	482	0.1	E
g	0.2	0.8	0.2	0.8	60	25	21	1.56×10^4	0.0176	0.05	318	0.2	M
h	0.8	0.2	0.2	0.8	54	21	21	1.56×10^4	0.0176	0.05	215	0.2	E
i	0.2	0.8	0.8	0.2	55	21	23	1.56×10^4	0.0176	0.05	893	0.3	\sim FE
j	0.8	0.2	0.8	0.2	53	26	28	1.56×10^4	0.0176	0.11	889	0.3	FE
k	0.2	0.8	0.2	0.8	59	30	34	1.56×10^4	0.0176	0.25	800	0.2	FE
l	1.0	0.0	0.0	1.0	44	49	39	1.56×10^4	0.0176	1.00	989	0.1	U
m	1.0	0.0	0.0	1.0	51	55	29	1.39×10^4	0.0159	1.00	870	0.5	U
n	1.0	0.0	0.0	1.0	57	43	34	1.56×10^4	0.0176	0.25	596	0.04	U
o	1.0	0.0	0.0	1.0	39	62	34	1.74×10^4	0.0193	4.00	1471	0.04	U

Table 1. Label of tested cases, initial concentration (mass basis) of each species within the target (ϕ_{1t} and ϕ_{2t}) and impact (ϕ_{1i} and ϕ_{2i}) piles, initial diameters of target and impact piles, D_t and D_i , respectively, initial separation Δx_d , channel Reynolds number Re , undisturbed shear velocity u_* , ratio between initial masses m_i/m_t , proposed timescale t_s (Eq. 4 in Subsection 3.3), characteristic time t_c (shown in Subsection 3.3), and interaction pattern Pat . C, M, E, FC, FE and U stand for chasing, merging, exchange, fragmentation-chasing, fragmentation-exchange and undefined patterns, respectively.

212 We followed the barchans consisting of bidisperse mixtures, for different concen-
 213trations of species 1 and 2, and we found patterns similar to those found by Assis and
 214Franklin (2020) for monodisperse (one-species) barchans. The obtained patterns are shown
 215in Figure 2 for fixed concentrations $\phi_1 = 0.5$ and $\phi_2 = 0.5$ in both initial piles (cases a
 216to e in Table 1), and in Figure 3 for concentrations ϕ_1 and ϕ_2 alternating between ei-
 217ther 0.2 or 0.8 (cases f to k in Table 1). Movies for all cases are available on an open
 218repository (Assis et al., 2021), and for cases b and o in the supporting information.

219 For $\phi_1 = \phi_2 = 0.5$, the same interaction patterns of one-species barchans occur (Assis
 220 & Franklin, 2020), namely the chasing, merging, exchange, fragmentation-chasing and

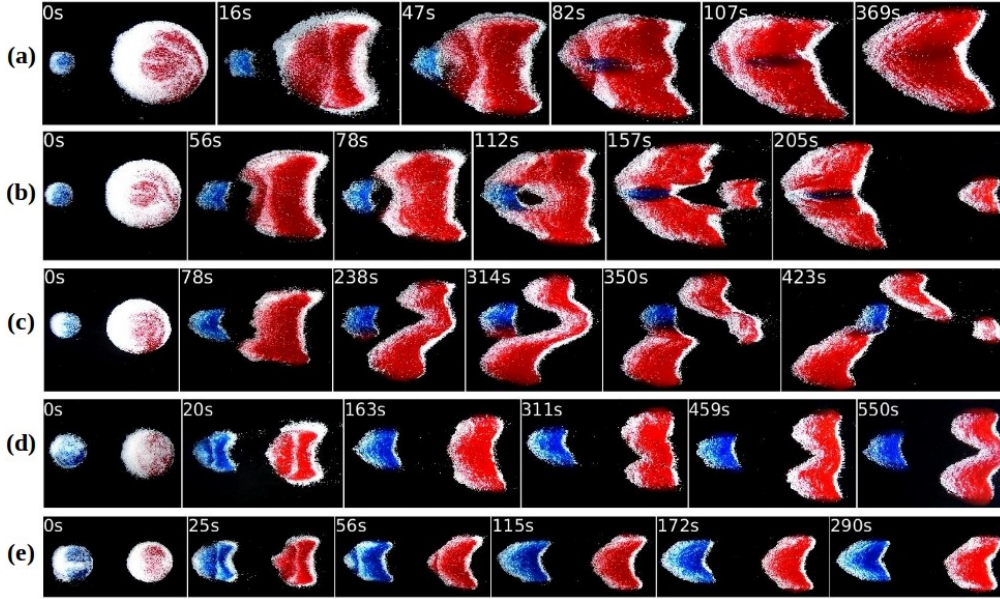


Figure 2. Snapshots of interactions of bidisperse barchans for fixed initial concentrations $\phi_1 = 0.5$ and $\phi_2 = 0.5$. In the snapshots, the white (clearer) beads correspond to $d_2 = 0.5$ mm and red and blue (darker) beads to $d_1 = 0.2$ mm, the water flow is from left to right, and the corresponding times are shown in each frame. Figures (a) to (e) correspond to cases *a* to *e* of Table 1: (a) merging; (b) exchange; (c) fragmentation-exchange; (d) fragmentation-chasing; (e) chasing.

221 fragmentation-exchange patterns (Figures 2e, 2a, 2b, 2d and 2c, respectively). By alter-
 222 nating ϕ_1 and ϕ_2 between either 0.2 or 0.8, using the same (Figures 3a, 3b, 3e and 3f,
 223 corresponding to cases *f*, *g*, *j* and *k* of Table 1) or inverted (Figures 3c and 3d, corre-
 224 sponding to cases *h* and *i* of Table 1) concentrations for the impact and target barchans,
 225 and for three values of m_i/m_t while all the other parameters were kept constant, we ob-
 226 tained the merging, exchange and fragmentation-exchange patterns. We note that it is
 227 probable that the chasing and fragmentation-chasing patterns exist also for the concen-
 228 trations employed. We did not, however, varied the mass ratio in order to seek for them.

229 Although the bidisperse piles (mixtures) produce the same interaction patterns ob-
 230 served for one-species barchans, they present some peculiarities in terms of morphody-
 231 namics. Two of them are related with grain segregation, as shown by Alvarez et al. (2021)
 232 for single barchans: the accumulation of the smaller grains over the surface of bedforms,
 233 and the appearance of a transient stripe, transverse to the flow direction, that initiates
 234 upstream the crest of the initial bedform and migrates toward its leading edge until dis-
 235 appearing. Alvarez et al. (2021) showed that the transient stripe separates the region
 236 where segregation is complete from that where segregation is ongoing, and the same fea-
 237 ture applies here since bidisperse conical piles are being deformed into bidisperse barchans.
 238 Another difference is the formation of a large void (absence of grains) when the impact
 239 barchan reaches the target one in the exchange pattern (Figures 2b and 3a, correspond-
 240 ing to cases *b* and *f* in Table 1). This void region occurs in the recirculation bubble of
 241 the impact barchan and persists until a baby barchan containing only grains from the
 242 target one is ejected. The baby barchan has roughly the same projected area of the im-
 243 pact barchan when $\phi_1 = \phi_2 = 0.5$, but not necessarily when $\phi_1 \neq \phi_2$, and, just after the
 244 baby barchan is ejected (at 157 s in Figure 2b and 155 s in Figure 3a), the parent bed-
 245 form has an unusual shape, resembling two elongated barchans containing grains from

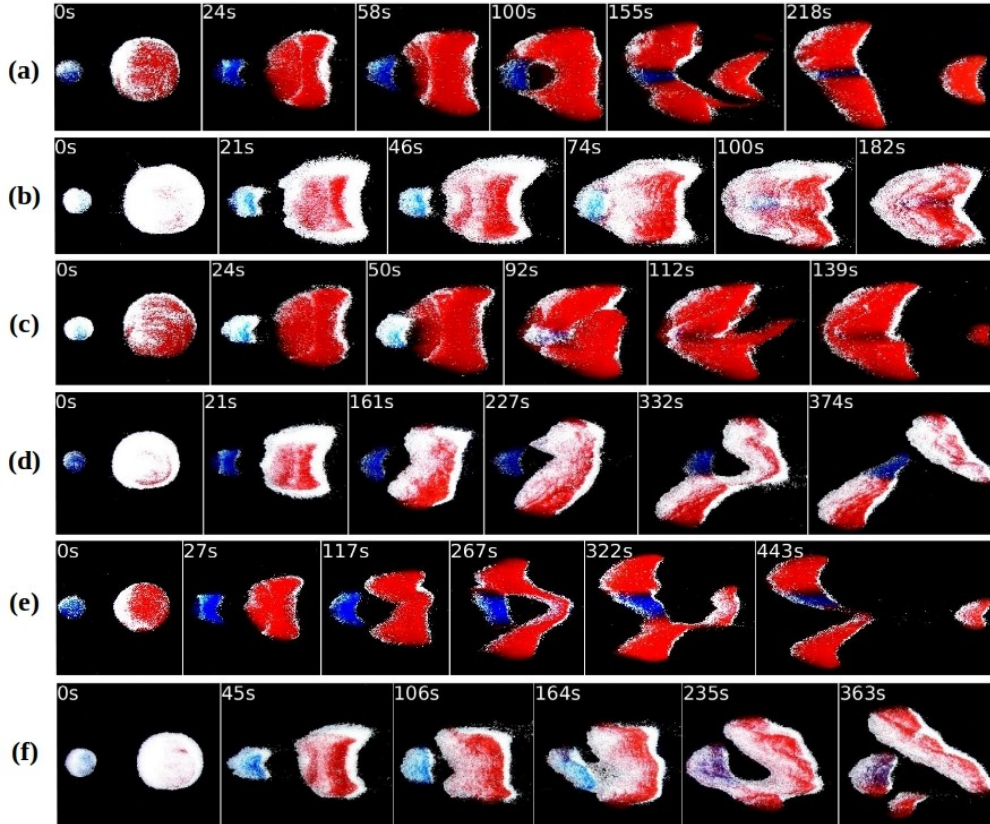


Figure 3. Snapshots of interactions of bidisperse barchans for fixed initial concentrations ϕ_1 and ϕ_2 alternating between either 0.2 or 0.8. In the snapshots, the white (clearer) beads correspond to $d_2 = 0.5$ mm and red and blue (darker) beads to $d_1 = 0.2$ mm, the water flow is from left to right, and the corresponding times are shown in each frame. Figures (a) to (f) correspond to cases f to k of Table 1: (a) exchange; (b) merging; (c) exchange; (d) fragmentation-exchange; (e) fragmentation-exchange; (f) fragmentation-exchange.

246
247

the target barchan and linked by grains from the impact one. After some time, the parent bedform attains a barchan shape.

248
249
250
251
252
253
254
255
256
257
258
259
260
261

Figure 4a presents the time evolution of areas occupied by the void region A_{vd} , normalized by the total area (projected area) A_t occupied by grains, for the exchange cases when $\phi_1 = \phi_2 = 0.5$ (Figure 2b, case b) and $\phi_1 \neq \phi_2$ (Figure 3a, case f). The computation of areas began when the impact barchan reached the target one, forming a closed void, and finished when the void was no longer closed, the baby barchan being ejected just afterward (see the supporting information for examples of void region detection and the time evolution of A_{vd} in dimensional form). We observe that the void area corresponds to 5 to 10% of the projected area occupied by the grains, the void remaining roughly constant for a certain time and then increasing considerably by the time the baby barchan is to be ejected. We observe also that the void is greater when in the presence of a large concentration of smaller grains. The reasons and mechanisms by which the void is formed remain to be investigated further, but they seem associated with granulometric distributions, since we had not observed voids in our experiments with one-species barchans (Assis & Franklin, 2020, 2021).

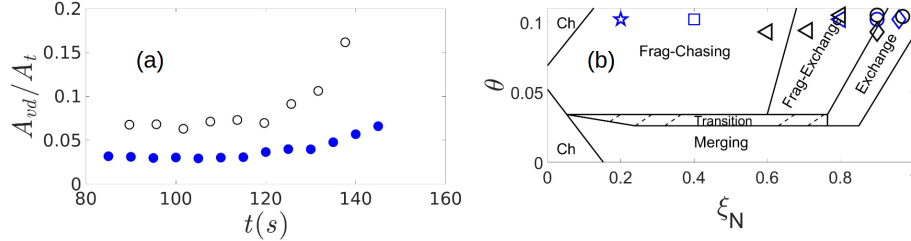


Figure 4. (a) Area occupied by the void region A_{void} normalized by the total area (projected) A_t occupied by grains as a function of time. Solid blue circles correspond to the exchange pattern when $\phi_1 = \phi_2 = 0.5$ (Figure 2b, case *b*) and open black symbols when $\phi_1 \neq \phi_2$ (Figure 3a, case *f*). (b) Interaction patterns for barchans of bidisperse mixtures: classification map proposed by Assis and Franklin (2020) for monodisperse barchans, over which we superposed the experimentally obtained chasing - Ch (\star), merging (\diamond), exchange (\circ), fragmentation-chasing (\square), and fragmentation-exchange (\triangleleft) patterns for the bidisperse case. Blue color corresponds to $\phi_1 = \phi_2 = 0.5$ (Figure 2) and black to $\phi_1 \neq \phi_2$ (Figure 3). Figure modified from Assis and Franklin (2020).

262 As a consequence of the differences aforementioned, the resulting patterns in the
 263 bidisperse case do not necessarily occur under the same conditions as for monodisperse
 264 barchans. Figure 4b plots the experimental points measured with bidisperse barchans
 265 in the map proposed by Assis and Franklin (2020) for the aligned case (figure modified
 266 from Assis & Franklin, 2020), which is drawn in the parameter space consisting of the
 267 Shields number θ and dimensionless particle number $\xi_N = \Delta_N/\Sigma_N$, where Δ_N is the dif-
 268 ference and Σ_N the sum of the number of grains forming each pile. For the bidisperse
 269 case (symbols in Figure 4b), θ of each pile was computed for each species (i.e., θ_1 and
 270 θ_2 using d_1 and d_2 , respectively) and then averaged by the number of grains of each species:
 271 $\theta = N_1\theta_1/N + N_2\theta_2/N$, where N_1 , N_2 and N are the number of grains of species 1, 2,
 272 and their sum, respectively. In addition, for cases where impact and target barchans had
 273 different compositions (cases *h* and *i*), θ was afterward computed as an averaged weighted
 274 by the size (total number of grains) of each barchan. We observe that most of points fall
 275 within the corresponding patterns found in the monodisperse case, or very near the bound-
 276 aries, but some of them deviate, crossing regions in the map. In general, while the ex-
 277 change, fragmentation-chasing and fragmentation-exchange tend to remain within their
 278 respective boundaries, the chasing and merging patterns deviate considerably, the former
 279 crossing the line and occupying part of the fragmentation-chasing region and the
 280 latter occupying part of the exchange region. We note that if we had used m_i/m_t or a
 281 length ratio (as other authors did, e.g., Endo et al., 2004; Katsuki et al., 2005, 2011; Génois,
 282 Hersen, et al., 2013) instead of ξ_N , many of the symbols would be superposed in Figure
 283 4b even if measured patterns are different, since the mass ratio does not take into con-
 284 sideration details about granular compositions. This corroborates, in a certain way, the
 285 use of a dimensionless parameter based on the number of elements (ξ_N) rather than m_i/m_t .

286 In particular, we analyzed the projected areas occupied by grains during some ex-
 287 change patterns. For monodisperse dunes, Assis and Franklin (2020, 2021) showed that
 288 the impact barchan first merges with the target one, and afterward a new barchan (baby
 289 barchan) is ejected (the remaining bedform being the parent barchan). In addition, Assis
 290 and Franklin (2020) showed that the baby barchan has roughly the same size of the im-
 291 pact barchan, but contains grains only from the target one. In the case of bidisperse mix-
 292 tures, a similar behavior happens. Figure 5 shows the projected areas of bedforms dur-
 293 ing the exchange processes of Figures 2b, 3a and 3c (cases *a*, *f* and *h*, corresponding to
 294 black, blue and red colors, respectively). A graphic in dimensional form is available in the

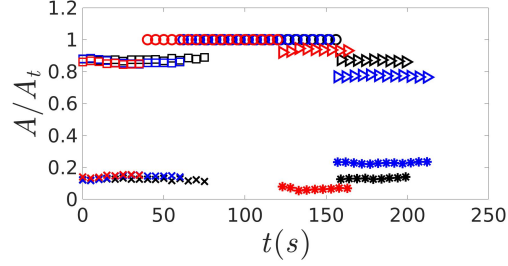


Figure 5. Projected areas, normalized by A_t , of impact (x), target (\square), merged (o), parent (\triangleright), and baby (*) barchans, respectively, as functions of time, during exchange processes. Black, blue and red colors correspond to cases *a*, *f* and *h* (Figures 2b, 3a and 3c), respectively.

295 supporting information). While the baby barchan does not contain grains from the impact
 296 impact barchan (seen directly from Figures 2b, 3a and 3c), Figure 5 shows that their areas
 297 are roughly the same (for the analyzed cases).

298 In summary, we show that in the mixed case the interaction patterns and their dynam-
 299 ics are roughly the same as in the monodisperse case; however, although the maps
 300 proposed in Assis and Franklin (2020) bring valuable information for classifying the barchan-
 301 barchan interactions, results with polydisperse dunes can deviate from the proposed bound-
 302 aries. Therefore, the distribution of grains within the barchans should be taken into con-
 303 sideration in analyses of barchan-barchan interactions occurring in nature.

304 **3.2 Two-species monodisperse piles**

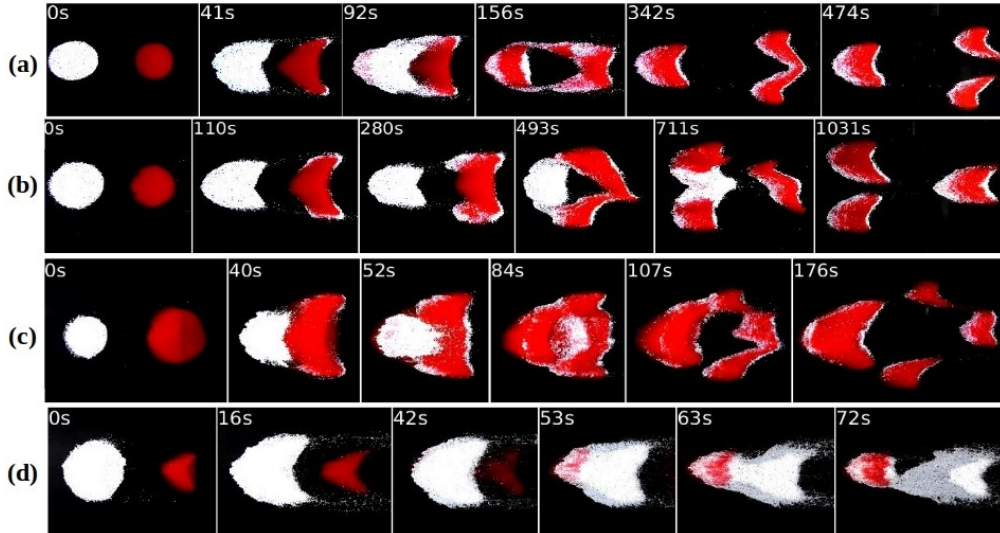


Figure 6. Snapshots of barchan interactions for initially monodisperse piles of different grains (two-species monodisperse piles). In the snapshots, the upstream pile consists of white (clearer) beads with $d_2 = 0.5$ mm and the downstream pile of red (darker) beads with $d_1 = 0.2$ mm, the water flow is from left to right, and the corresponding times are shown in each frame. Figures (a) to (d) correspond to cases *l* to *o* of Table 1.

305 We followed the initially monodisperse bedforms consisting each of different grains,
 306 and we found different patterns. These patterns, cases *l* to *o* in Table 1, are shown in
 307 Figure 6, which presents snapshots of barchans at some instants during their interactions,
 308 including a collision where the impact barchan was larger than the target one (see the
 309 supporting information or Assis et al. (2021) for movies of collisions). For this specific
 310 case, we made use of larger grains in the impact dune since the displacement velocity
 311 of barchans varies with the diameter of their grains (Franklin & Charru, 2011, see also
 312 Eq. 2 in Subsection 3.3).

313 For all the interactions shown in Figure 6, the impact barchan consisted of grains
 314 of species 2 ($d_2 = 0.5$ mm) in white color and the target barchan of species 1 ($d_1 = 0.2$
 315 mm) in red color. In Figure 6a (case *l* in Table 1), the barchans collide, forming a large
 316 void in the recirculation region when they touch each other, and with the larger grains
 317 moving over the smaller ones that, in their turn, emerge at the toe of the resulting bed-
 318 form (at 92 s). Afterward (at 156 s), the smaller grains having accumulated over the sur-
 319 face of the resulting bedform, the latter begins to split in what seems, initially, two barchans
 320 linked by two large branches. Finally (at 474s), they split in three barchans (one upstream
 321 and two downstream, in a staggered configuration) consisting each of bidisperse grains.
 322 Figures 7a and 7b show the time evolution of projected areas of dunes for cases *l* and
 323 *m*, respectively (Figures 7c and 7d in dimensionless form, normalized by A_t). Interest-
 324 ingly, we can observe from Figure 7a that, after the dunes collide (at ~ 90 s), the pro-
 325 jected area of the resulting bedform first increases and then decreases. This is due, res-
 326 pectively, to larger grains migrating over the smaller ones and spreading over the dune,
 327 and afterward the smaller grains accumulating over the dune surface and decreasing the
 328 projected area. In addition, Figure 7a shows that the two final downstream barchans have
 329 roughly the same size.

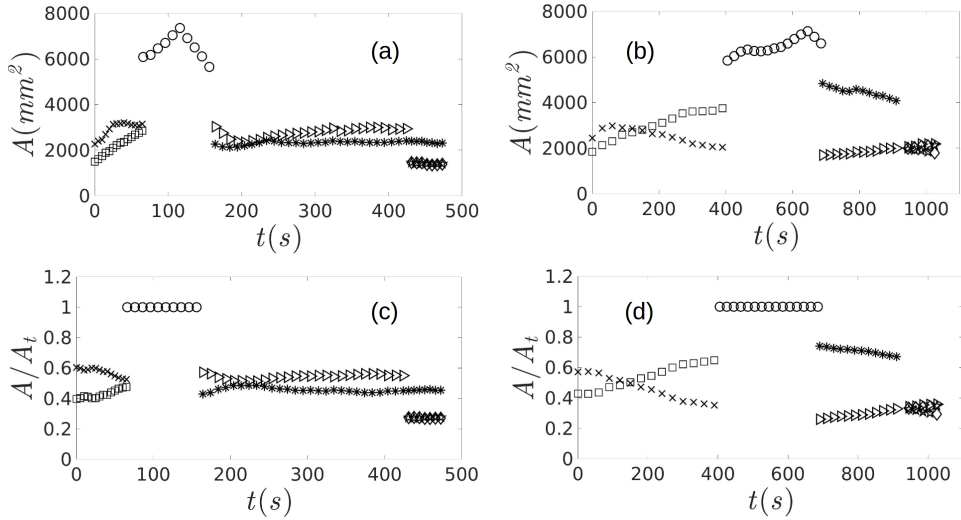


Figure 7. Projected areas of impact (x), target (\square), merged (\circ), upstream after splitting (*), parent (\diamond), and baby barchans (\star), respectively, during undefined-exchange processes for (a) and (c) case *l* (Figure 6a) and (b) and (d) case *m* (Figure 6b). Figures (a) and (b) are in dimensional and (c) and (d) in dimensionless form (normalized by A_t).

330 In Figure 6b (case *m* in Table 1), the behavior is similar to that of Figure 6a, the
 331 main difference being that the final state is inverted: two upstream barchans and one
 332 downstream barchan, in a staggered configuration. In both cases *l* and *m* the initial masses

333 are the same (the initial diameter of the impact pile being larger since it consists of larger
 334 grains), only the fluid velocity is different, being higher for case *l*. Why the behavior changes
 335 by changing the water velocity remains to be investigated (we do not advance an expla-
 336 nation for the moment). However, we can observe from Figure 7b the same increase and
 337 decrease of the projected area after the dunes have collided (at ~ 400 s), that the resul-
 338 tant bedform splits first in one larger upstream and one smaller downstream bedform
 339 (at ~ 700 s), and that the upstream bedform splits in two dunes later (at ~ 950 s). We
 340 end finally with three barchans of roughly the same size.

341 Figure 6c corresponds to case *n* of Table 1, and shows a collision in which three barchans
 342 are ejected from the merged bedform. This case resembles the exchange pattern (Assis
 343 & Franklin, 2020, 2021), with the difference that three baby barchans are ejected, one
 344 aligned and two in staggered configuration.

345 Finally, Figure 6d corresponds to case *o* of Table 1, the unusual case of a collision
 346 of a larger impact with a smaller target barchan (as far as we know, this is the first time
 347 that this kind of collision is reported. See the supporting information or Assis et al. (2021)
 348 for a movie of this interaction). We observe that, as the impact barchan gets closer to
 349 the target one, the latter becomes more elongated, while grains leaving the horns of the
 350 impact barchan are entrained further downstream and are not incorporated by the tar-
 351 get barchan. During the collision ($t \approx 48$ s), the larger grains move over the smaller ones,
 352 which, in their turn, emerge at the toe of the resulting bedform. Finally, a monodisperse
 353 baby barchan consisting of only larger grains is ejected from the merged bedform (grains
 354 from the impact dune, different from all cases reported previously), resulting, in fact, of
 355 larger grains being entrained further downstream. The remaining grains form an upstream
 356 bidisperse barchan with smaller grains populating its upper surface.

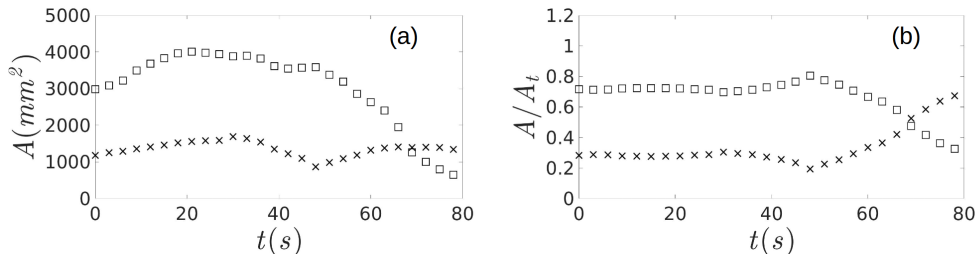


Figure 8. Time evolution of projected areas occupied by white (\square) and red (\times) grains for case *o* (Figure 6d), in (a) dimensional form and (b) normalized by A_t . OBS: the monolayer consisting of white grains observed in Figure 6d was neglected.

357 Figure 8 shows the time evolution of projected areas occupied by white and red grains
 358 for case *o*. From Figure 8a, we observe an initial increase of both areas due to the spread-
 359 ing of the initial conical pile (being deformed into barchan dunes), with a time interval
 360 when areas remain roughly constant. When the larger dune approaches the smaller one,
 361 the vortex on the recirculation region of the former entrains grains from the latter to-
 362 ward its lee face. Because the larger grains move easier over the smaller ones (Alvarez
 363 et al., 2021), these remain on the bottom of the impact barchan until they emerge at the
 364 toe of the impact one, being again exposed to the fluid flow. When the dunes collide,
 365 the white grains then move over the red (smaller) ones, which appear at the toe of the
 366 resulting bedform. This “swallowing” process appears in Figure 8 as a decrease followed
 367 by an increase of the area occupied by red grains within $30 \text{ s} < t < 70 \text{ s}$. Finally, by the
 368 end of the collisional process ($t \approx 70$ s on), a greater number of larger (white) grains are
 369 exposed to the fluid flow and are either entrained further downstream or form a mono-

370 layer between both barchans, which makes the area occupied by the larger (white) grains
 371 to decrease considerably (the monolayer being neglected in Figure 8).

372 In common for cases *l* to *o*, the larger grains move over the smaller ones, being en-
 373 trained further downstream and/or accumulating on the lee face and forming a carpet
 374 for the smaller grains. The same mechanism proposed by Alvarez et al. (2021) seems to
 375 apply here, i.e., the segregation results from a competition between fluid entrainment
 376 and easiness of rolling. Other than that, we do not advance more explanations for the
 377 patterns shown in Figure 6, but we propose, however, a timescale that applies to all cases
 378 investigated and is presented in Subsection 3.3.

379 3.3 Timescale

380 A question that remained to be answered for barchan-barchan interactions even
 381 in monodisperse conditions (Endo et al., 2004; Hersen & Douady, 2005; Assis & Franklin,
 382 2020, 2021), and that can now be investigated for bidisperse barchans, is the existence
 383 of a proper timescale for the problem. A reasonable timescale for the binary interaction
 384 of dunes can be built as their initial separation Δx_d divided by their relative velocity ΔV_d ,

$$t_s = \frac{\Delta x_d}{\Delta V_d} \quad (1)$$

385 where ΔV_d is the difference between the displacement velocities V_d of impact and tar-
 386 get barchans. t_s represents a typical time for the collision of barchans (faster for closer
 387 barchans with stronger relative velocities). Franklin and Charru (2011) investigated the
 388 displacement velocities of subaqueous barchans by varying water velocities, grain types,
 389 and dune sizes, and found that they vary as

$$\frac{V_d}{V_{ref}} \sim \frac{d}{L} (\theta - \theta_{th})^n \quad (2)$$

390 where d is the mean grain diameter, L is the barchan length, θ_{th} is the threshold value
 391 of the Shields number for incipient motion, n is an exponent, and $V_{ref} = ((S-1)gd)^{1/2}$,
 392 with $S = \rho_s/\rho$. Observing that the diameter of the initial pile D is proportional to L ,
 393 and considering the mean diameter and density as in Alvarez et al. (2021), $\bar{d} = (\phi_1/d_1 + \phi_2/d_2)^{-1}$
 394 and $\bar{\rho}_s = \phi_1\rho_1 + \phi_2\rho_2$, respectively, we obtain

$$\Delta V_d \sim u_* \left| \frac{\bar{d}_t}{D_t} - \frac{\bar{d}_i}{D_i} \right| \frac{1}{S} \quad (3)$$

395 where \bar{d}_i and \bar{d}_t represent the mean diameter of grains forming impact and target barchans,
 396 respectively, and D_i and D_t are the initial diameters of the projected areas of impact
 397 and target bedforms, respectively. Finally,

$$t_s = \frac{\Delta x_d S}{u_*} \left| \frac{\bar{d}_t}{D_t} - \frac{\bar{d}_i}{D_i} \right|^{-1} \quad (4)$$

398 By normalizing the time interval that barchans take to complete their interaction
 399 Δt by the proposed timescale t_s , we obtain the characteristic time for interactions $t_c =$
 400 $\Delta t/t_s$ (values shown in Table 1). The initial instant for Δt is when the flow starts and
 401 the final instant when the interaction reaches a stage characteristic of the considered pat-
 402 tern. In cases with collision (merging, exchange and fragmentation-exchange), the final
 403 instant is when collision takes place, and in cases without collision (chasing and fragmentation-
 404 chasing), the final time is much larger than the duration of tests and we consider Δt as

405 tending to infinity. In general, we observe the following characteristic times for interac-
 406 tions:

- 407 • $0.04 \leq t_c < 2$ for cases with collisions, i.e., the merging, exchange, fragmentation-
 408 exchange (by considering also the one-species monodisperse barchans presented
 409 in Assis and Franklin (2020, 2021)) and the undefined patterns of the two-species
 410 monodisperse barchans;
- 411 • $t_c = \infty$ for the chasing and fragmentation-chasing patterns.

412 Because only cases *n* and *o* (two-species monodisperse barchans) present $t_c = 0.04$
 413 < 0.1 and only one fragmentation-exchange pattern for one-species monodisperse barchans
 414 (Assis & Franklin, 2021) presents $t_c = 1.7 > 1$, we obtained, in general, that $t_c = O(0.1)$,
 415 where $O()$ stands for "order of magnitude". This characteristic time holds for the barchans
 416 of same monodisperse composition (one species) presented in Assis and Franklin (2020,
 417 2021), for the barchans consisting of bidisperse mixtures, and for the barchans consist-
 418 ing of different monodisperse grains.

419 If the proposed timescale proves to be valid for other environments, it will allow
 420 the prediction of durations of barchan-barchan interactions and, more generally, provide
 421 a scaling for the evolution of dune fields on terrestrial deserts and other planetary en-
 422 vironments.

423 4 Conclusions

424 In this paper, we investigated experimentally the dune-dune interactions for barchans
 425 consisting of (i) bidisperse mixtures and (ii) different monodisperse grains (one type for
 426 each barchan). The experiments were conducted in a water channel where two barchans
 427 interacted with each other while filmed by a camera, and the bedform morphologies and
 428 duration of interactions were obtained from image processing. We observed that a tran-
 429 sient stripe appears over the dunes in cases of bidisperse mixtures (as also happens for
 430 single bidisperse barchans, Alvarez et al., 2021), that interaction patterns vary with con-
 431 centrations, and that different interactions exist when each barchan consists of differ-
 432 ent monodisperse grains (two-species monodisperse barchans). For the latter, we obtained,
 433 for the first time, one very peculiar case by using larger grains in the impact barchan:
 434 the collision of a larger upstream barchan with a smaller downstream one, which showed
 435 a different grain distribution in the resulting bedform once the collision had taken place.
 436 Finally, we proposed a timescale for the interactions of both monodisperse and bidisperse
 437 barchans (cases i and ii, and also one-species monodisperse barchans). The identifica-
 438 tion of such timescale represents a new step for predicting the duration of binary inter-
 439 actions and, more generally, scaling the evolution of dune fields on Earth, Mars and other
 440 planetary environments.

441 Acknowledgments

442 The authors are grateful to FAPESP (Grant Nos. 2016/18189-0,
 443 2018/14981-7 and 2019/10239-7) for the financial support provided. Data
 444 supporting this work are available in the supporting information and in
 445 <http://dx.doi.org/10.17632/sbjtzbzh9k>.

446 References

- 447 Alvarez, C. A., Cúñez, F. D., & Franklin, E. M. (2021). Growth of barchan dunes of
 448 bidispersed granular mixtures. *Phys. Fluids*, *33*(5), 051705.
- 449 Alvarez, C. A., & Franklin, E. M. (2017, Dec). Birth of a subaqueous barchan

- dune. *Phys. Rev. E*, *96*, 062906. Retrieved from <https://link.aps.org/doi/10.1103/PhysRevE.96.062906> doi: 10.1103/PhysRevE.96.062906
- Assis, W. R., Cúñez, F. D., & Franklin, E. M. (2021). Experimental data on barchan-barchan interaction with bidisperse grains. *Mendeley Data*, <http://dx.doi.org/10.17632/sbjtzbzh9k>.
- Assis, W. R., & Franklin, E. M. (2020). A comprehensive picture for binary interactions of subaqueous barchans. *Geophys. Res. Lett.*, *47*(18), e2020GL089464.
- Assis, W. R., & Franklin, E. M. (2021). Morphodynamics of barchan-barchan interactions investigated at the grain scale. *J. Geophys. Res.: Earth Surf.*, *126*(8), e2021JF006237.
- Bacik, K. A., Lovett, S., Caulfield, C.-c. P., & Vriend, N. M. (2020, Feb). Wake induced long range repulsion of aqueous dunes. *Phys. Rev. Lett.*, *124*, 054501. Retrieved from <https://link.aps.org/doi/10.1103/PhysRevLett.124.054501> doi: 10.1103/PhysRevLett.124.054501
- Bagnold, R. A. (1941). *The physics of blown sand and desert dunes*. London: Chapman and Hall.
- Bo, T. L., & Zheng, X. J. (2013). Collision behaviors of barchans in aeolian dune fields. *Environ. Earth. Sci.*, *70*, 2963-2970.
- Bristow, N. R., Blois, G., Best, J. L., & Christensen, K. T. (2018). Turbulent flow structure associated with collision between laterally offset, fixed-bed barchan dunes. *J. Geophys. Res.-Earth*, *123*(9), 2157-2188.
- Bristow, N. R., Blois, G., Best, J. L., & Christensen, K. T. (2019). Spatial scales of turbulent flow structures associated with interacting barchan dunes. *J. Geophys. Res.-Earth*, *124*(5), 1175-1200.
- Bristow, N. R., Blois, G., Best, J. L., & Christensen, K. T. (2020). Secondary flows and vortex structure associated with isolated and interacting barchan dunes. *J. Geophys. Res.-Earth*, *125*(2), e2019JF005257.
- Claudin, P., & Andreotti, B. (2006). A scaling law for aeolian dunes on Mars, Venus, Earth, and for subaqueous ripples. *Earth Plan. Sci. Lett.*, *252*, 20-44.
- Crocker, J. C., & Grier, D. G. (1996). Methods of digital video microscopy for colloidal studies. *Journal of Colloid and Interface Science*, *179*(1), 298-310.
- Durán, O., Schwämmle, V., & Herrmann, H. (2005, Aug). Breeding and solitary wave behavior of dunes. *Phys. Rev. E*, *72*, 021308. Retrieved from <https://link.aps.org/doi/10.1103/PhysRevE.72.021308> doi: 10.1103/PhysRevE.72.021308
- Durán, O., Schwämmle, V., Lind, P. G., & Herrmann, H. (2009). The dune size distribution and scaling relations of barchan dune fields. *Granular Matter*, *11*, 7-11.
- Elbelrhiti, H., Andreotti, B., & Claudin, P. (2008). Barchan dune corridors: Field characterization and investigation of control parameters. *Journal of Geophysical Research: Earth Surface*, *113*(F2).
- Elbelrhiti, H., Claudin, P., & Andreotti, B. (2005). Field evidence for surface-wave-induced instability of sand dunes. *Nature*, *437*(04058).
- Endo, N., Taniguchi, K., & Katsuki, A. (2004). Observation of the whole process of interaction between barchans by flume experiments. *Geophys. Res. Lett.*, *31*(12).
- Franklin, E. M., & Charru, F. (2009). Morphology and displacement of dunes in a closed-conduit flow. *Powder Technology*, *190*, 247-251.
- Franklin, E. M., & Charru, F. (2011). Subaqueous barchan dunes in turbulent shear flow. Part 1. Dune motion. *J. Fluid Mech.*, *675*, 199-222.
- Gay, S. P. (1999). Observations regarding the movement of barchan sand dunes in the nazca to tanaca area of southern peru. *Geomorphology*, *27*(3), 279 - 293.
- Génois, M., du Pont, S. C., Hersen, P., & Grégoire, G. (2013). An agent-based model of dune interactions produces the emergence of patterns in deserts. *Geophys. Res. Lett.*, *40*(15), 3909-3914.

- 505 Génois, M., Hersen, P., du Pont, S., & Grégoire, G. (2013). Spatial structuring
506 and size selection as collective behaviours in an agent-based model for barchan
507 fields. *Eur. Phys. J. B*, *86*(447).
- 508 Herrmann, H. J., & Sauermann, G. (2000). The shape of dunes. *Physica A (Amster-*
509 *dam)*, *283*, 24-30.
- 510 Hersen, P. (2004). On the crescentic shape of barchan dunes. *Eur. Phys. J. B*,
511 *37*(4), 507–514.
- 512 Hersen, P., Andersen, K. H., Elbelrhiti, H., Andreotti, B., Claudin, P., & Douady,
513 S. (2004, Jan). Corridors of barchan dunes: Stability and size selection. *Phys.*
514 *Rev. E*, *69*, 011304. Retrieved from [https://link.aps.org/doi/10.1103/](https://link.aps.org/doi/10.1103/PhysRevE.69.011304)
515 [PhysRevE.69.011304](https://link.aps.org/doi/10.1103/PhysRevE.69.011304) doi: 10.1103/PhysRevE.69.011304
- 516 Hersen, P., & Douady, S. (2005). Collision of barchan dunes as a mechanism of size
517 regulation. *Geophys. Res. Lett.*, *32*(21).
- 518 Hersen, P., Douady, S., & Andreotti, B. (2002, Dec). Relevant length
519 scale of barchan dunes. *Phys. Rev. Lett.*, *89*, 264301. Retrieved from
520 <https://link.aps.org/doi/10.1103/PhysRevLett.89.264301> doi:
521 [10.1103/PhysRevLett.89.264301](https://link.aps.org/doi/10.1103/PhysRevLett.89.264301)
- 522 Hugenholtz, C. H., & Barchyn, T. E. (2012). Real barchan dune collisions and ejections.
523 *Geophys. Res. Lett.*, *39*(2).
- 524 Katsuki, A., Kikuchi, M., Nishimori, H., Endo, N., & Taniguchi, K. (2011). Cellular
525 model for sand dunes with saltation, avalanche and strong erosion: collisional
526 simulation of barchans. *Earth Surf. Process. Landforms*, *36*(3), 372-382.
- 527 Katsuki, A., Nishimori, H., Endo, N., & Taniguchi, K. (2005). Collision dynamics of
528 two barchan dunes simulated using a simple model. *J. Phys. Soc. Jpn.*, *74*(2),
529 538-541.
- 530 Kocurek, G., Ewing, R. C., & Mohrig, D. (2010). How do bedform patterns arise?
531 new views on the role of bedform interactions within a set of boundary condi-
532 tions. *Earth Surf. Process. Landforms*, *35*(1), 51-63.
- 533 Lima, A., Sauermann, G., Herrmann, H., & Kroy, K. (2002). Modelling a dune field.
534 *Physica A*, *310*(3), 487-500. Retrieved from [https://www.sciencedirect](https://www.sciencedirect.com/science/article/pii/S0378437102005460)
535 [.com/science/article/pii/S0378437102005460](https://www.sciencedirect.com/science/article/pii/S0378437102005460)
- 536 Norris, R. M., & Norris, K. S. (1961). Algodones Dunes of Southeastern California.
537 *GSA Bulletin*, *72*(4), 605-619.
- 538 Parteli, E., & Herrmann, H. (2003). A simple model for a transverse dune field.
539 *Physica A*, *327*(3), 554-562.
- 540 Parteli, E. J. R., & Herrmann, H. J. (2007, Oct). Dune formation on the present
541 mars. *Phys. Rev. E*, *76*, 041307. Retrieved from [https://link.aps.org/doi/](https://link.aps.org/doi/10.1103/PhysRevE.76.041307)
542 [10.1103/PhysRevE.76.041307](https://link.aps.org/doi/10.1103/PhysRevE.76.041307) doi: 10.1103/PhysRevE.76.041307
- 543 Schlichting, H. (2000). *Boundary-layer theory*. New York: Springer.
- 544 Schwämmle, V., & Herrmann, H. J. (2003). Solitary wave behaviour of sand dunes.
545 *Nature*, *426*, 619-620.
- 546 Vermeesch, P. (2011). Solitary wave behavior in sand dunes observed from space.
547 *Geophys. Res. Lett.*, *38*(22).
- 548 Zheng, X. J., Bo, T. L., & Zhu, W. (2009). A scale-coupled method for simulation
549 of the formation and evolution of aeolian dune field. *Int. J. Nonlinear Sci. Numer. Simul.*, *10*(3), 387-396.
- 550 Zhou, X., Wang, Y., & Yang, B. (2019). Three-dimensional numerical simulations of
551 barchan dune interactions in unidirectional flow. *Particul. Sci. Technol.*, *37*(7),
552 835-842.
553

Figure 1.

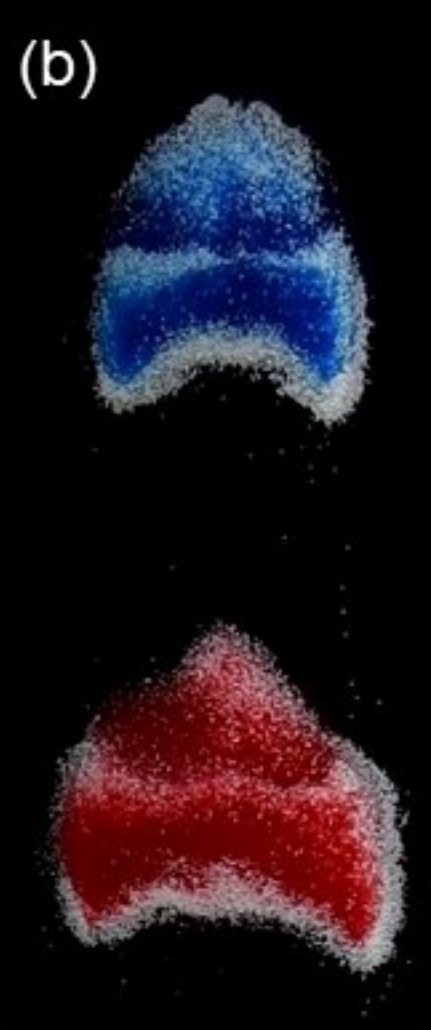
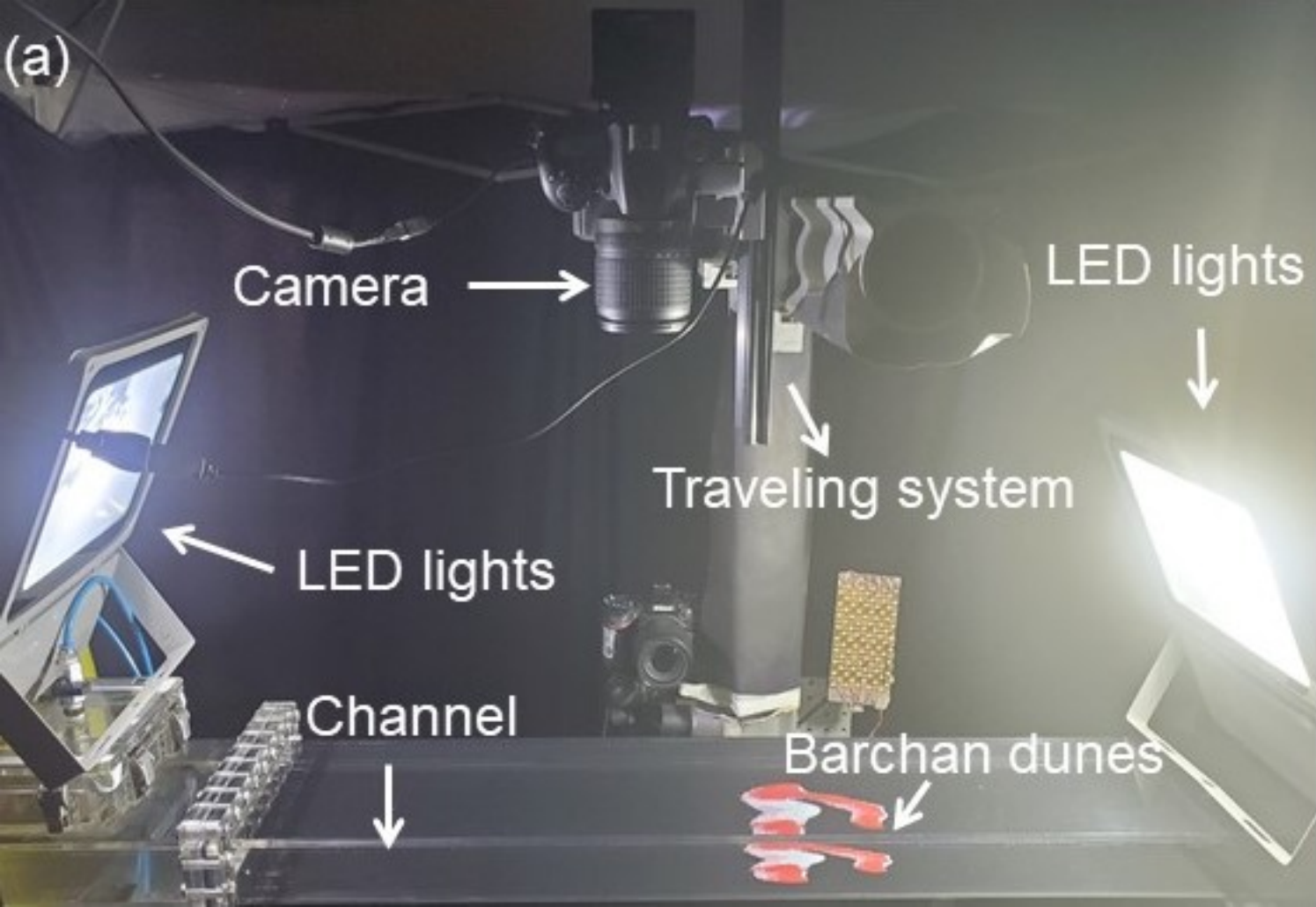


Figure 2.

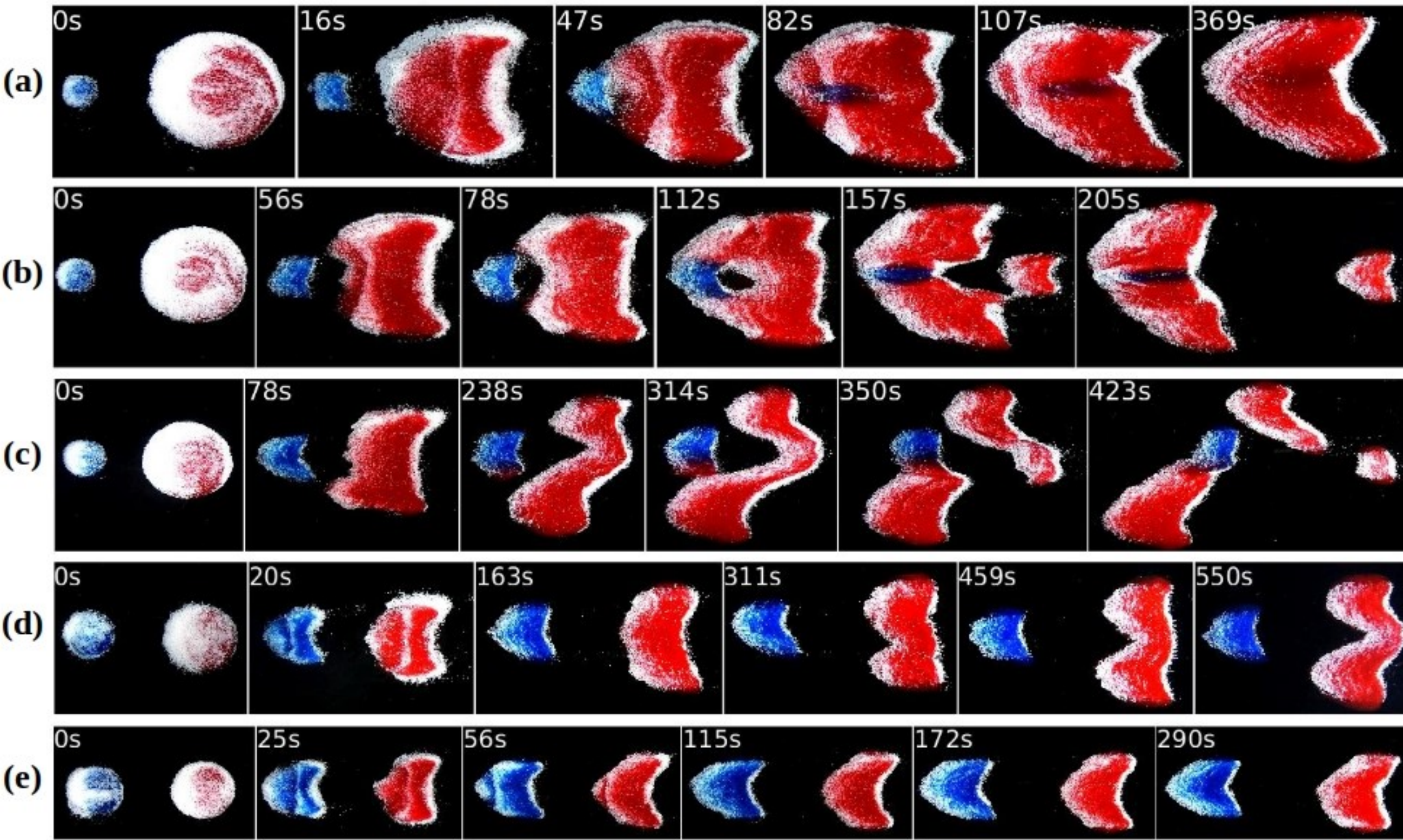


Figure 3.

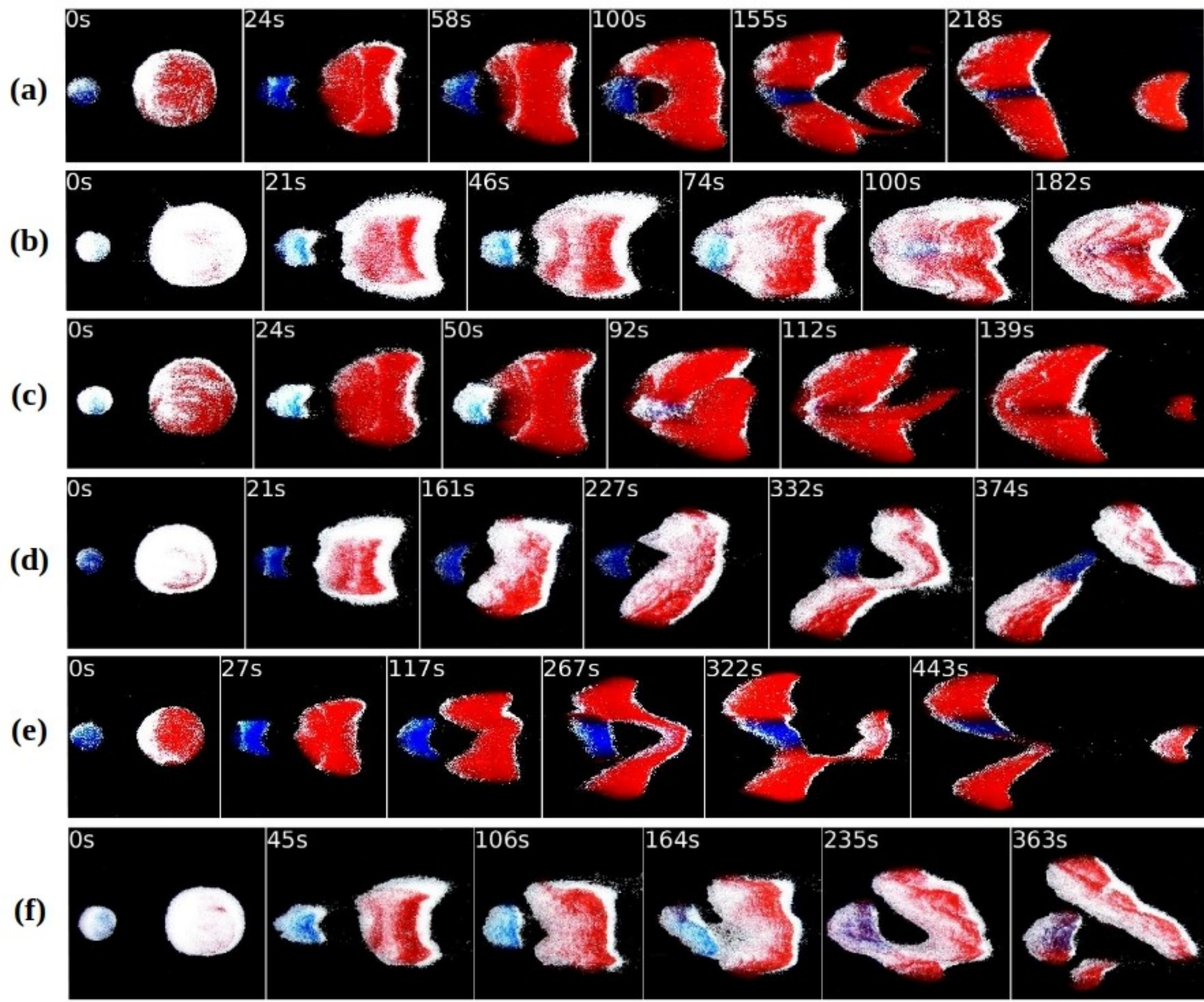


Figure 4.

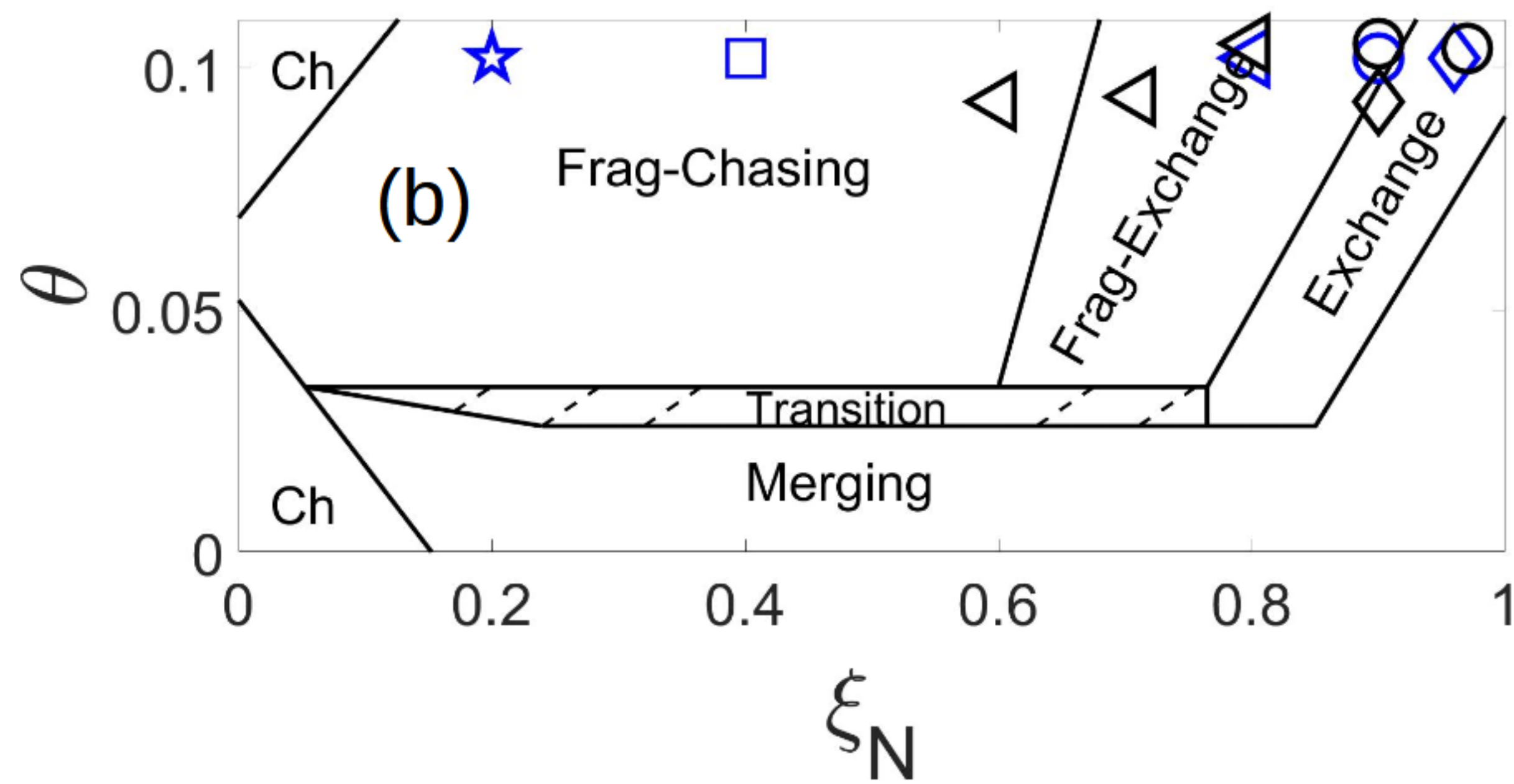
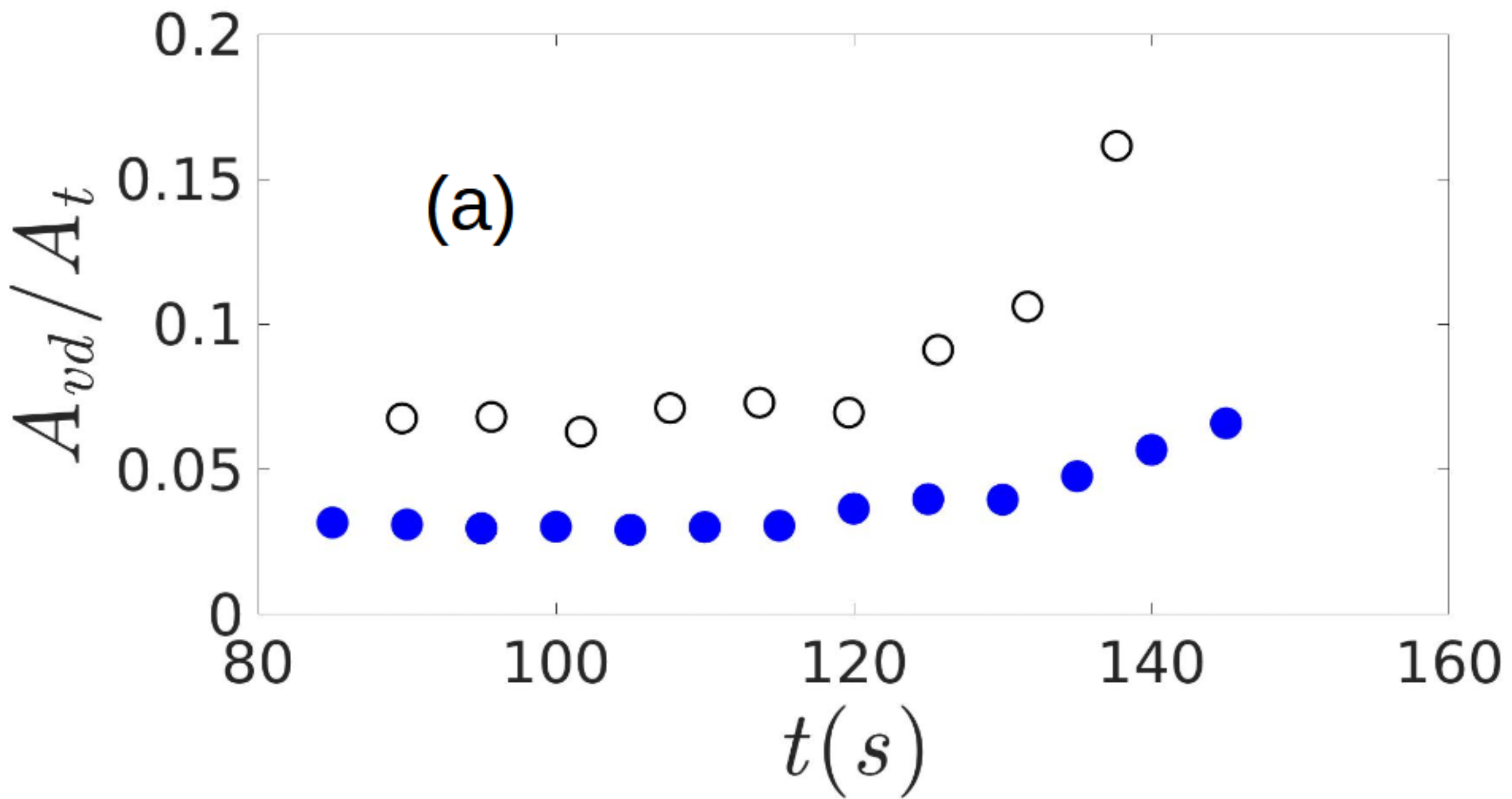


Figure 5.

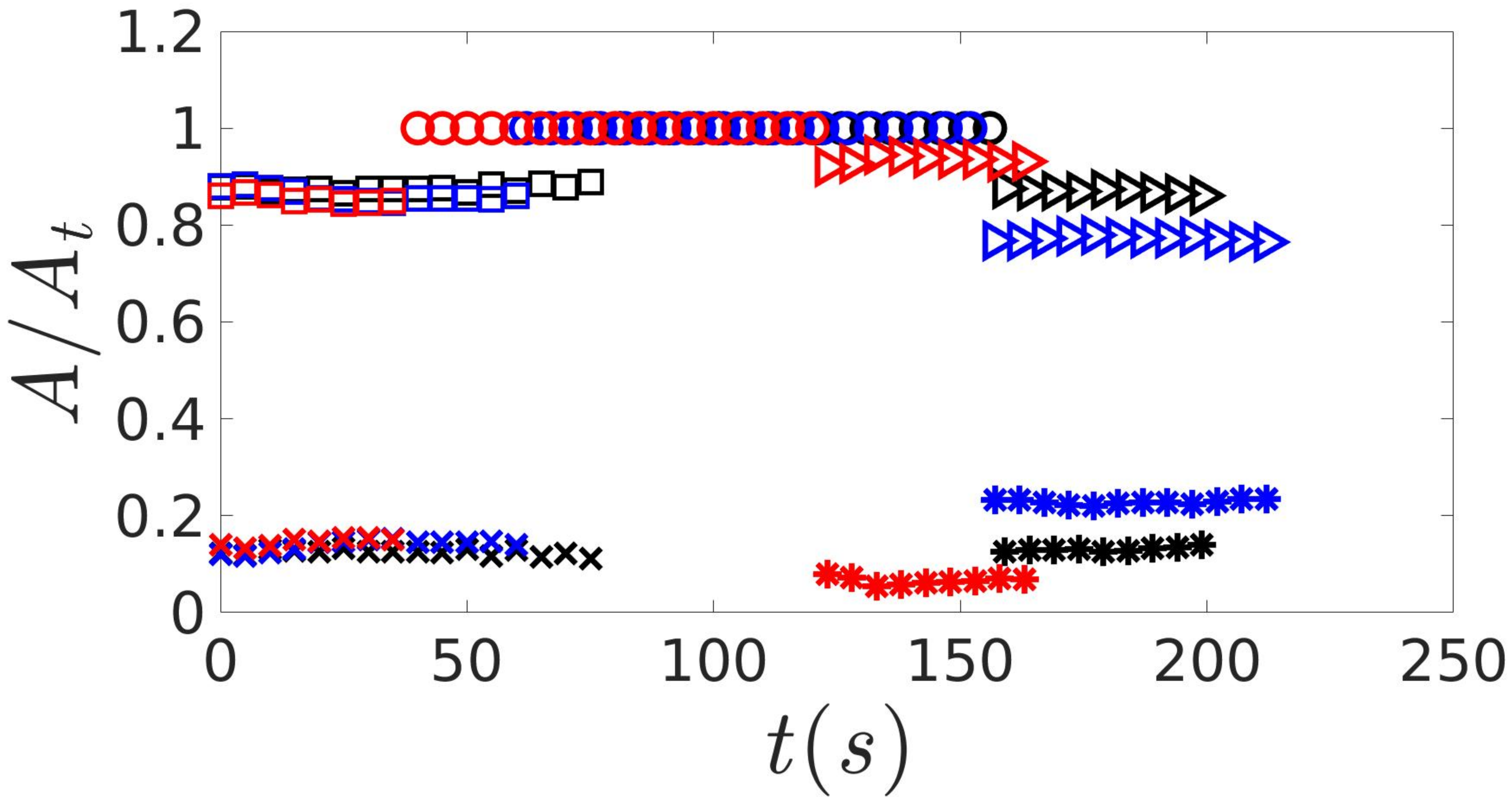


Figure 6.

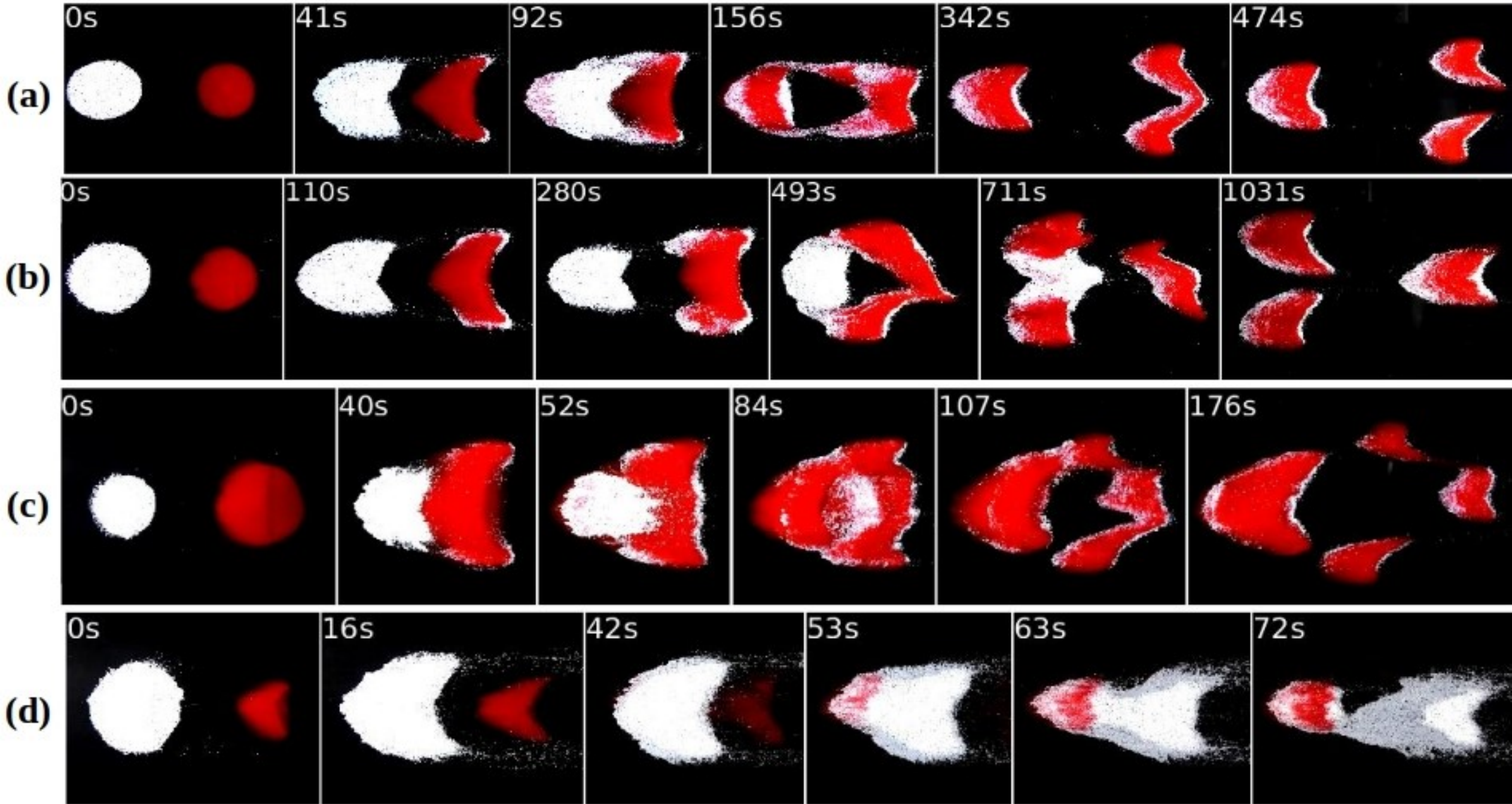


Figure 7.

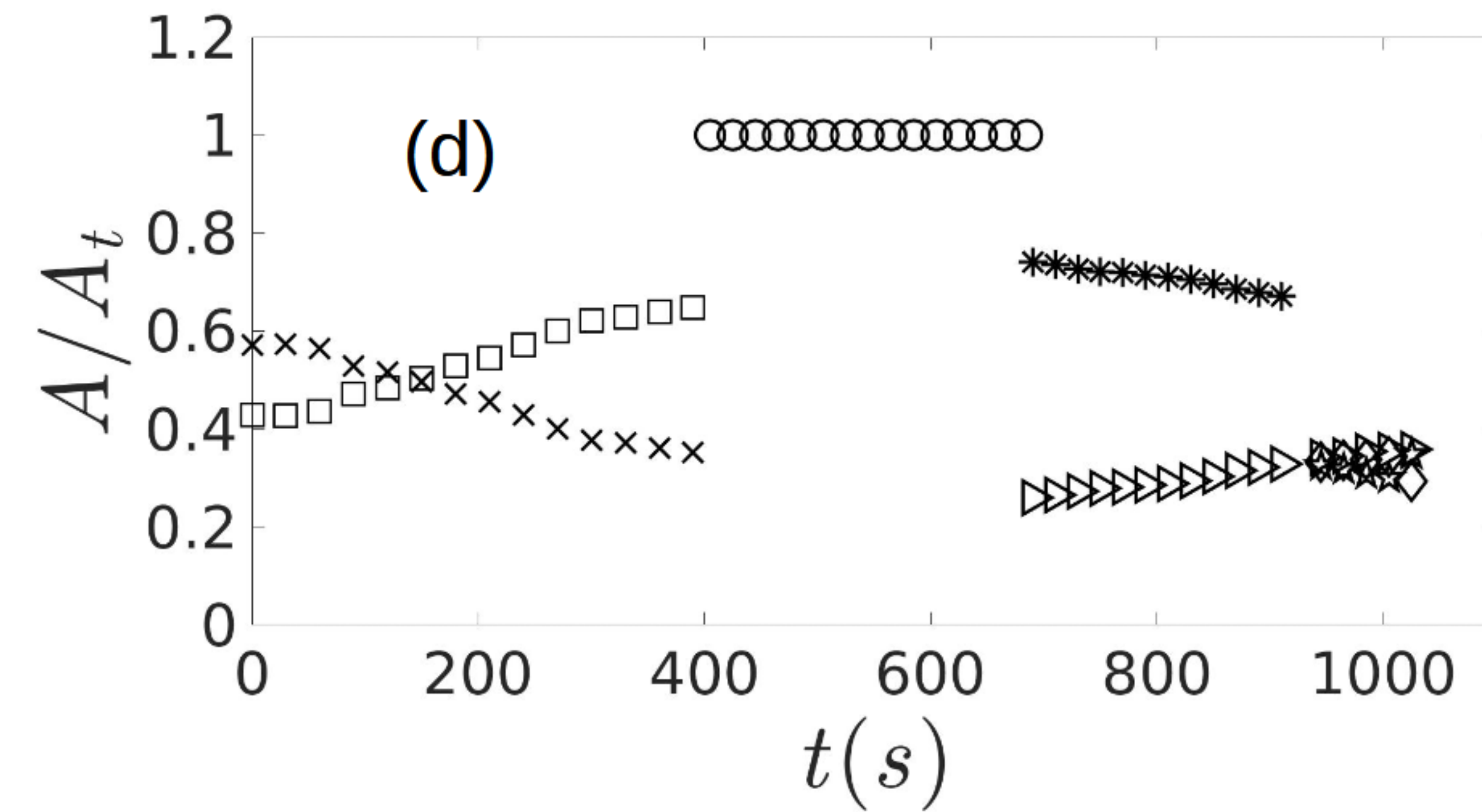
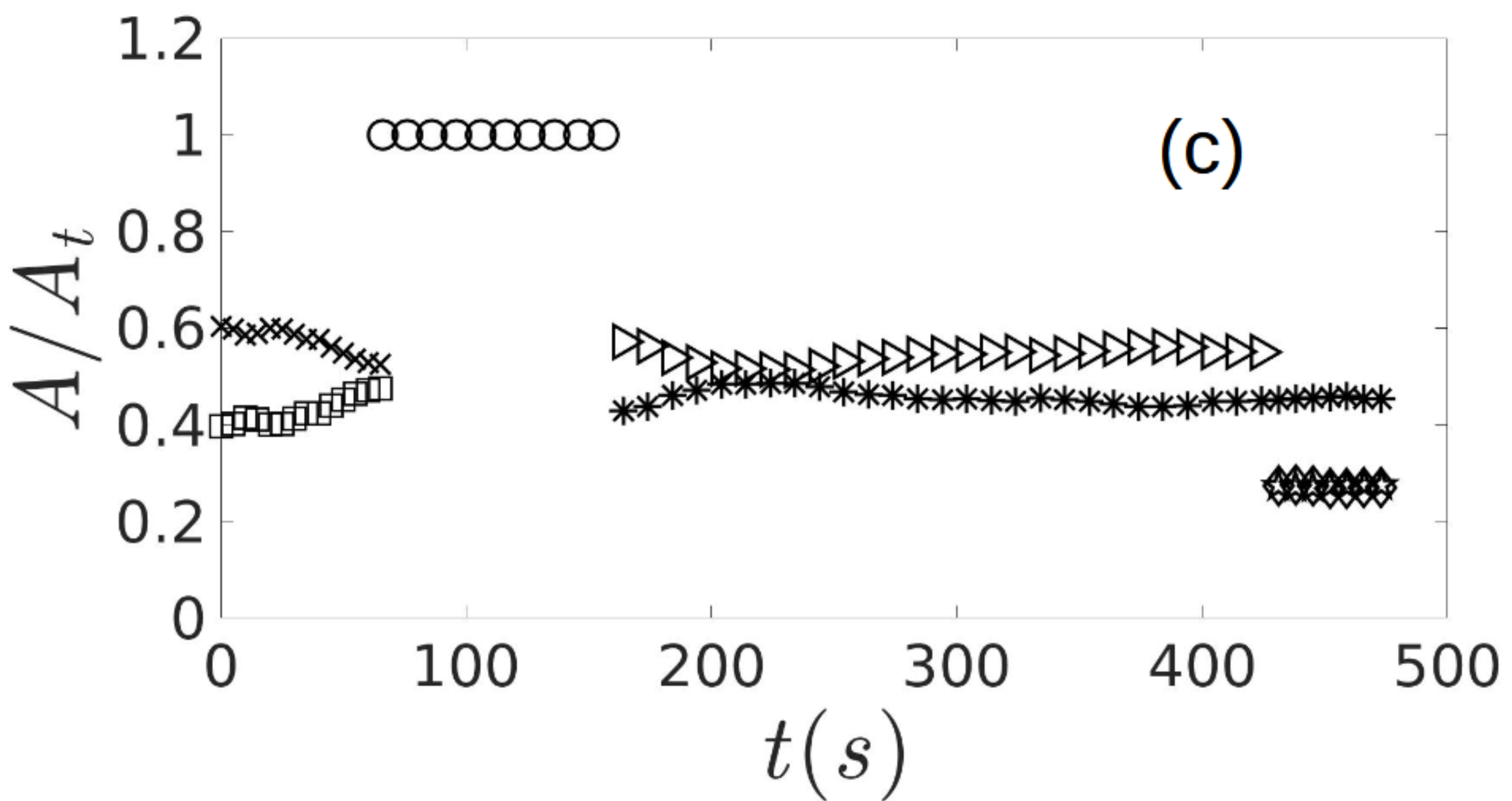
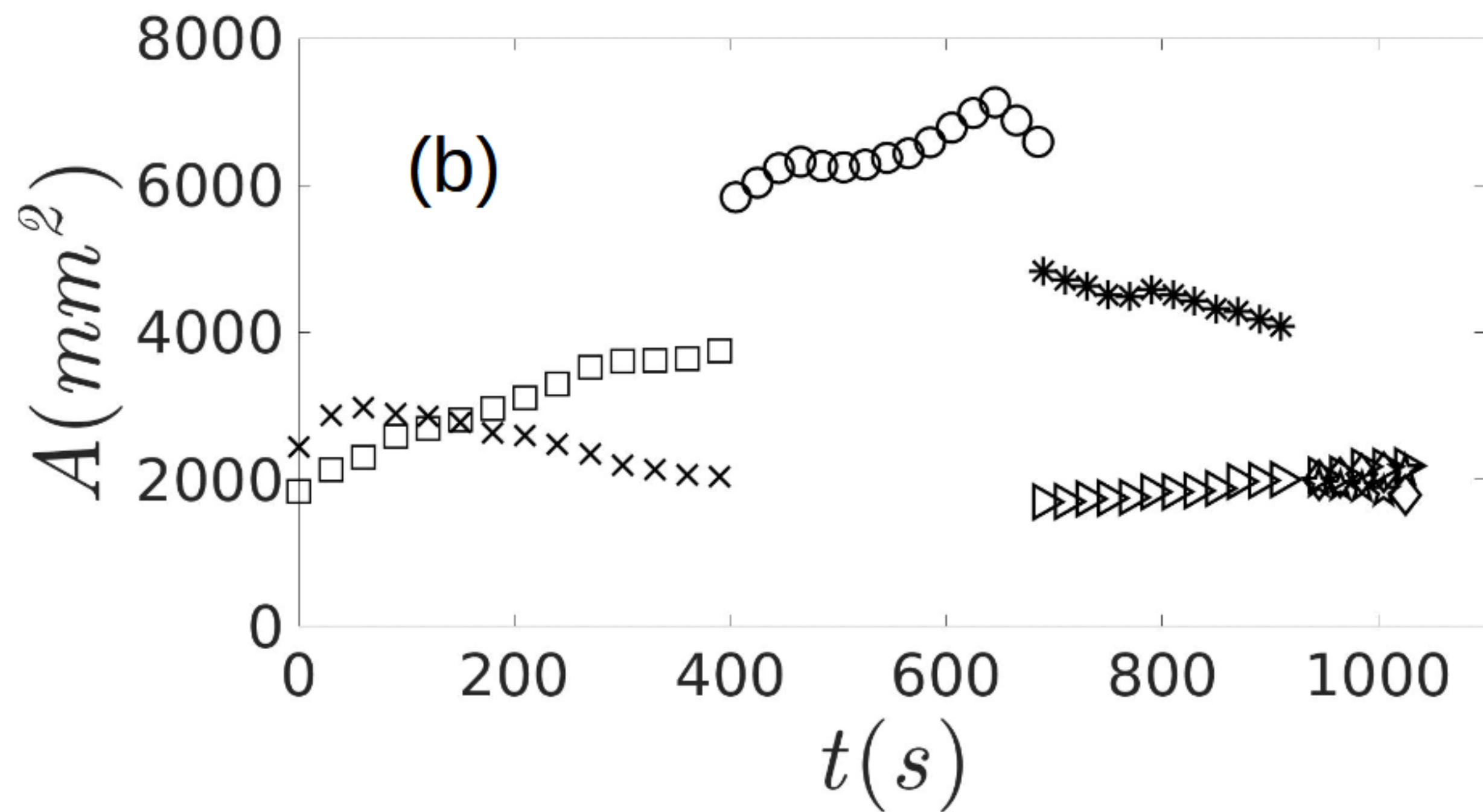
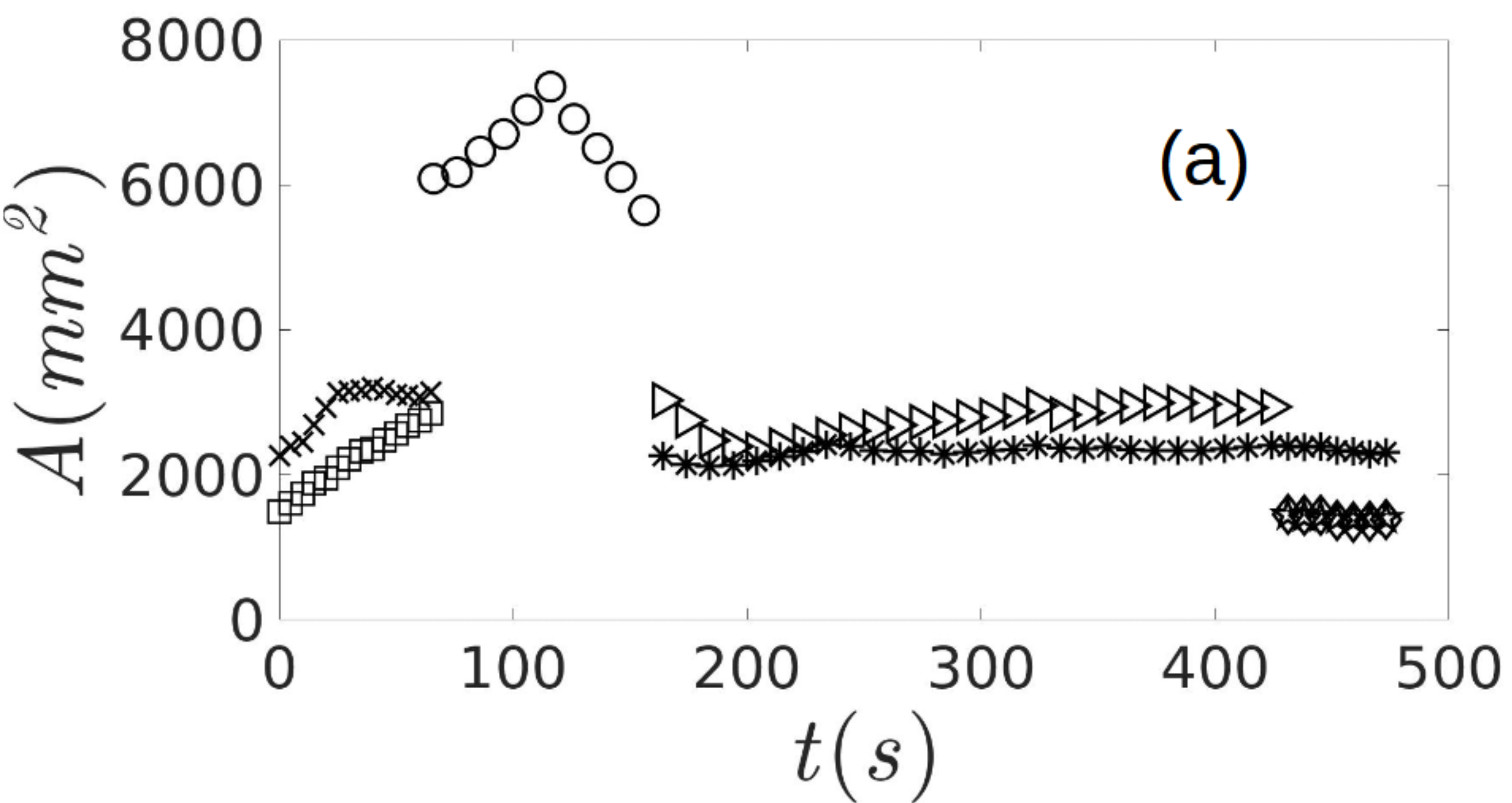


Figure 8.

